Sustainable Energy & Fuels

ROYAL SOCIETY OF CHEMISTRY

PAPER

View Article Online
View Journal | View Issue

Cite this: *Sustainable Energy Fuels*, 2025, **9**, 1545

The Achilles' heel of batteries with alkali metal electrodes†

Anna Michalak and M. Anji Reddy *

Received 4th December 2024
Accepted 30th January 2025

DOI: 10.1039/d4se01698j

rsc.li/sustainable-energy

There is a strong drive to use Li and Na metals as anode materials for lithium and sodium batteries due to their high specific energy. However, Li and Na metals are susceptible to dendrite growth and exhibit low melting points (180.5 °C for Li and 98 °C for Na). The low melting points can lead to internal short-circuits and catastrophic failure of the battery. Here, we show that batteries using Li and Na metal electrodes are short-circuiting internally when the melting points of these metals are reached. We demonstrated this with four different solid electrolytes in lithium and sodium batteries, using symmetric-, half-, and anode-free cells and through extensive impedance measurements and direct visualisation *via operando* digital microscopy. The temperature required to melt these metals in batteries is often reached under various operating conditions. In light of these facts, using Li and Na metals as electrodes in commercial batteries should be reconsidered.

Introduction

With a high standard reduction potential of −3.04 (*vs.* SHE) and a specific capacity of 3860 mA h g^{-1}, Li metal is an ideal anode for lithium-ion batteries (LIBs).[1] However, Li metal forms dendrites upon repeated deposition and stripping, eventually puncturing the polymeric separator, and the battery will short-circuit internally.[2,3] This could lead to thermal runaway, potential fire and explosion. To address this issue with Li metal, commercial LIBs use graphite-based anodes. Though the specific capacity (372 mA h g^{-1}) of graphite is 10 times less than that of Li metal, graphite offers higher safety and cycling stability than Li metal.[4,5] However, there is a significant demand for high-specific capacity anodes to increase the specific energy of LIBs. The silicon anode with a high specific capacity of 4212 mA h g^{-1} is attractive, but the high-volume changes of the Si anode during lithiation and delithiation are challenging to deal with.[6] Beyond this, the Li anode is necessary for Li-deficient battery technologies such as lithium–sulphur and lithium–air and desirable for high-energy and safer solid-state batteries.[7] Considering these specific needs for Li metal anodes, significant progress has been made to prevent Li dendrite formation and propagation.[8–10] On the other hand, hard carbon is used as an anode in sodium-ion batteries (SIBs),[11,12] as Na metal poses problems like Li metal. Nevertheless, Na metal as an anode is desirable due to its higher capacity (1115 mA h g^{-1} for Na *versus* 270 mA h g^{-1} for hard carbon) and for Na-deficient battery technologies.[13] Beyond this, there is a strong intention to develop anode-free batteries due to their higher energy density.[14,15] Unlike traditional LIBs and SIBs, anode-free batteries do not have anodes to start with; they only have an anode current collector. Li or Na metal is deposited on the current collector as an anode during the first charge, and it subsequently works as an anode material.[16] The anode current collector does not have a pre-coated anode material (reducing weight and manufacturing cost). So, the anode-free design offers higher energy density and is considered next-generation battery technology.[17]

While these are the exciting features of Li and Na as anodes, some fundamental issues are associated with Li and Na metals when they are used as anodes for LIBs and SIBs. Li melts at 180.5 °C, and Na melts at 98 °C.[18] When these temperatures are reached in batteries, Li and Na metals will melt and lead to an internal short circuit (as they are good electrical conductors), which might eventually lead to a thermal runaway.[19] Here, we show that batteries using Li and Na metals as electrodes lead to an internal short circuit when the temperature of the battery reaches the melting point of these metals. We demonstrate that internal short circuits can occur in LIBs and SIBs using four different solid electrolytes (2 for LIBs and 2 for SIBs). We investigated and reported the short-circuiting tendency using symmetrical cells, half-cells, and anode-free cells using various relevant experiments.

We opted for solid electrolytes rather than liquid electrolytes to demonstrate the short-circuiting behaviour of LIBs and SIBs. The commonly used liquid electrolytes in LIBs and SIBs are unstable at the melting temperatures of Li and Na metals. The stability of the electrolytes is paramount to demonstrate the short-circuiting behaviour. Any parasitic side reactions between

IMPACT Energy Storage Laboratory, Faculty of Science and Engineering, Swansea University, Fabian Way, Swansea SA1 8EN, UK. E-mail: a.r.munnangi@swansea.ac.uk

† Electronic supplementary information (ESI) available. See DOI: https://doi.org/10.1039/d4se01698j

the electrolytes and Li and Na metals should not influence the melting of these metals, and therefore, we have chosen stable solid electrolytes. We have chosen $Li_{6.4}La_3Zr_{1.4}Ta_{0.6}O_{12}$ (LLZO) and Li-β″-alumina (LBASE) as Li^+ conducting and Na-β″-alumina (BASE) and $Na_5GdSi_4O_{12}$ (NGS) as Na^+ conducting solid electrolytes. These solid electrolytes are chemically stable with respective metals (LLZO and LBASE against Li; BASE and NGS against Na).

Symmetric cells

Initially, we demonstrated the short-circuiting behaviour of symmetric cells. Fig. 1a and c show the impedance spectra (Nyquist plots) of Cu–Li/LLZO/Li–Cu and Cu–Li/LBASE/Li–Cu cells between 100 °C and 200 °C. The specific impedance values are given in Table S1.† The impedance spectra of these cells are composed of a single depressed semi-circle without any inclined line at lower frequencies. This is a typical behaviour expected for this kind of symmetrical cell. However, the Cu–Li/LBASE/Li–Cu cell impedance is significantly higher than that of Cu–Li/LLZO/Li–Cu. This could be due to the low ionic conductivity of LBASE compared to LLZO. This resulted in lower impedance for Cu–Li/LLZO/Li–Cu cells. Nevertheless, the impedance of both cells decreased with an increase in temperature due to the increased ionic conductivity and improved interfacial contact between the solid electrolyte and Li. The impedance of Cu–Li/LLZO/Li–Cu fell below 1 Ω at 190 °C. The impedance of Cu–Li/LBASE/Li–Cu fell below 1 Ω at 200 °C, confirming the short-circuiting tendency of these cells when Li metal started meting (above 180.5 °C) (Fig. 1b and d). We additionally confirmed the short-circuiting behaviour of these cells with a multimeter continuity test.

Fig. 2a and c show the Nyquist plots of Al–Na/BASE/Na–Al and Al–Na/NGS/Na–Al cells between 40 °C and 110 °C. The specific impedance values are given in Table S2.† The Al–Na/BASE/Na–Al cell impedance spectra comprise a single depressed semi-circle without any inclined line at lower frequencies. On the other hand, the impedance spectra of the Al–Na/NGS/Na–Al

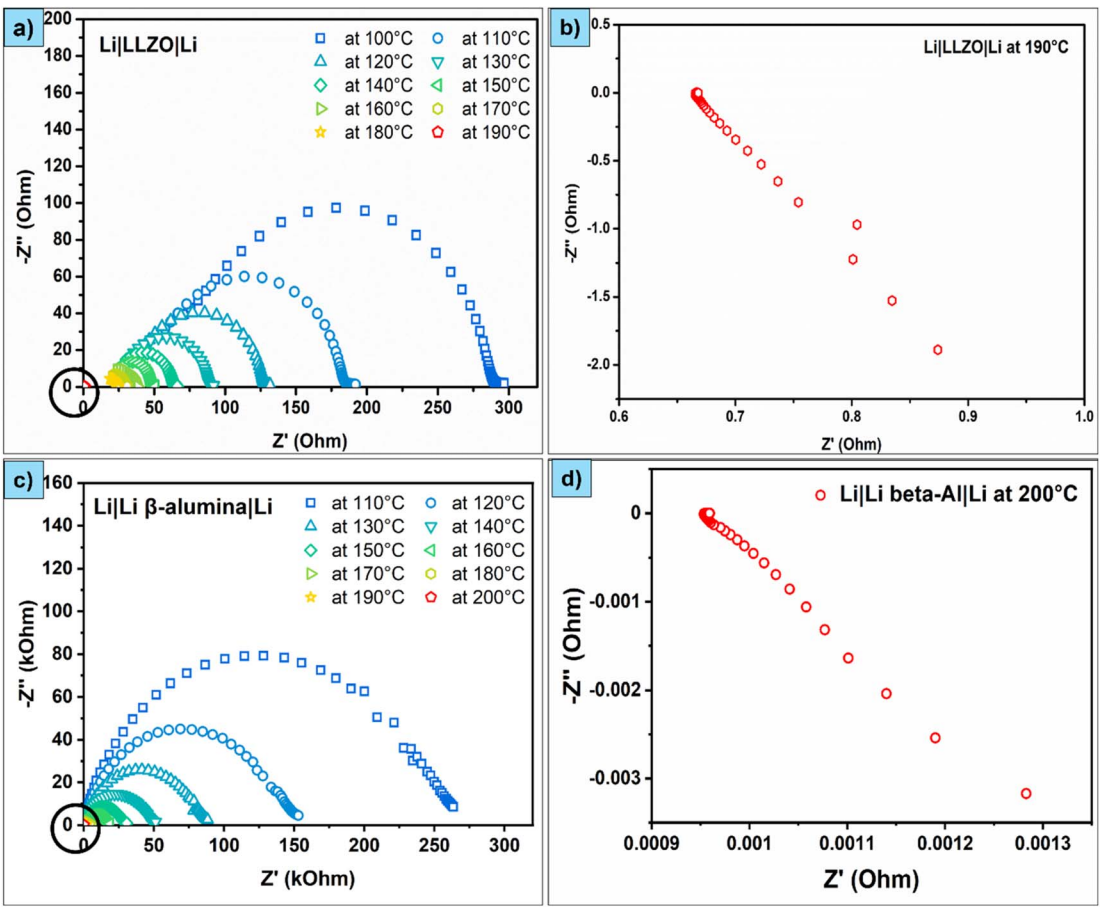

Fig. 1 (a) Impedance spectra of a Cu–Li/LLZO/Li–Cu cell in the temperature range of 100 °C to 190 °C with increments of +10 °C (the cell is equilibrated for at least 30 minutes at each temperature); (b) impedance spectra of the Cu–Li/LLZO/Li–Cu cell at 190 °C; (c) impedance spectra of a Cu–Li/LBASE/Li–Cu cell in the temperature range of 110 °C to 200 °C with increments of +10 °C; (d) impedance spectra of the Cu–Li/LBASE/Li–Cu cell at 200 °C. The red circles in (a) and (c) highlight the impedance falling below 1 Ω after short-circuiting occurs. The thickness of the solid electrolyte discs is between 1 and 1.2 mm, and their diameter is 11 to 12 mm. The weight of Li foil attached to the solid electrolyte disc on each side is approximately 10 mg. Impedance spectra were recorded in potentiostatic mode in the 0.1 Hz to 1 MHz frequency range. A small amplitude of 5 mV was applied to avoid significant metal deposition and stripping during the impedance measurements.

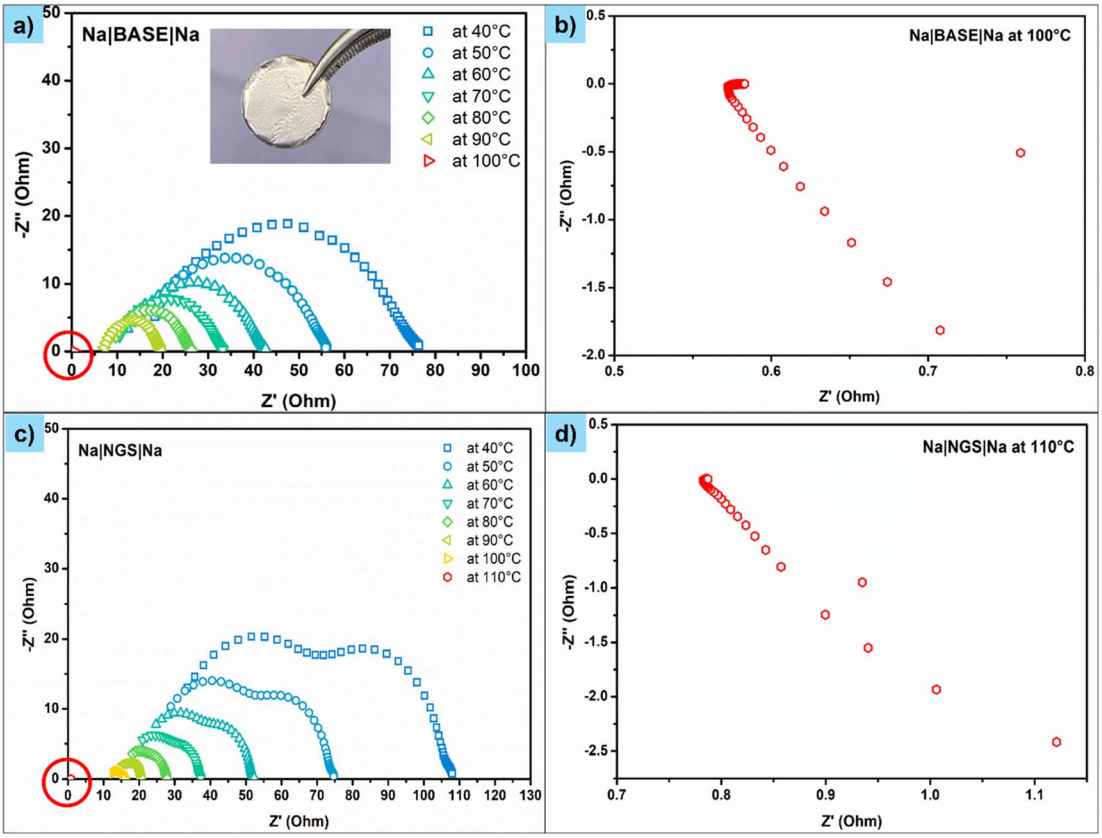

Fig. 2 (a) Impedance spectra of the Al–Na/BASE/Na–Al cell in the temperature range of 40 °C to 100 °C with increments of +10 °C; (b) impedance spectra of the Al–Na/BASE/Na–Al cell at 100 °C; (c) impedance spectra of the Al–Na/NGS/Na–Al cell in the temperature range of 40 °C to 110 °C with increments of +10 °C; (d) impedance spectra of the Al–Na/NGS/Na–Al cell at 110 °C. The red circle in (a) and (c) highlights the impedance falling below 1 Ω after short-circuiting occurs. The inset of (a) shows the digital image of a typical symmetrical cell.

cell are composed of two depressed semi-circles (disappear when the temperature increases) without any inclined line at lower frequencies. The two semicircles (instead of one) could be due to the slightly uneven surface of NGS or the uneven sticking of Na metal to the NGS surface on either side of the disc. In contrast to Li-based symmetric cells (Cu–Li/LLZO/Li–Cu and Cu–Li/LBASE/Li–Cu), the impedance of Na-based symmetric cells (Al–Na/BASE/Na–Al and Al–Na/NGS/Na–Al) is almost the same due to the similar ionic conductivity of NGS and BASE. Similar to Li-based cells, the impedance of Al–Na/BASE/Na–Al and Al–Na/NGS/Na–Al cells fell below 1 Ω between 100 and 110 °C just above the melting point of Na metal (98 °C) (Fig. 2b and d). Again, this confirms the short-circuiting behaviour of these cells when melting point temperature of Na metal is reached.

The short-circuiting temperature is 190 °C for LLZO and 200 °C for LBASE, which is close to the melting point of Li (180.5 °C). The short-circuiting temperature is 100 °C for BASE and 110 °C for NGS, which is close to the melting point of Na (98 °C). The slight variation in the short-circuiting temperature between the solid electrolytes could be related to the thickness and density of the solid electrolyte discs used. We used 1.0–1.2 mm thick solid electrolyte discs to physically separate the electrodes and to avoid accidental short-circuits when fabricating the cells. However, the intended thickness of the solid electrolyte is less than 50 μm for commercial cells. A 10 to 20 μm thick polymeric separator is used in liquid electrolyte cells. Given the low physical separation of electrodes in commercial batteries and pores within the solid electrolytes and/or separators, the melts will flow in the pores and lead to short-circuits even if the quantity of metal is low and at the melting temperatures of metals.

Impedance fell below 1 Ω when a short circuit occurred in all symmetric cells, irrespective of the electrode type and solid electrolyte used. While this is expected to happen when a short circuit occurs, interestingly, all the impedance spectra showed an inclined line with a negative imaginary impedance when a short circuit occurs (Fig. 1b, d, 2b and d, even in half-cells, Fig. 3b and d). This unusual impedance behaviour is generally observed when a shunt resistor is formed. A shunt is a resistor with low resistance, enabling high currents to pass through it. When an internal short circuit occurs in the cell, the current changes its direction of flow (external circuit to direct), and it creates low resistance paths due to the high electronic conductivity of the metals (1.1×10^7 S m^{-1} for Li and 2.1×10^7 S m^{-1} for Na), creating a shunt resistor. We recorded the impedance spectra of a shunt resistor to validate this (30 mΩ). The impedance spectra of the shunt resistor resemble those of the short-circuited cells (Fig. S1†). A similar impedance

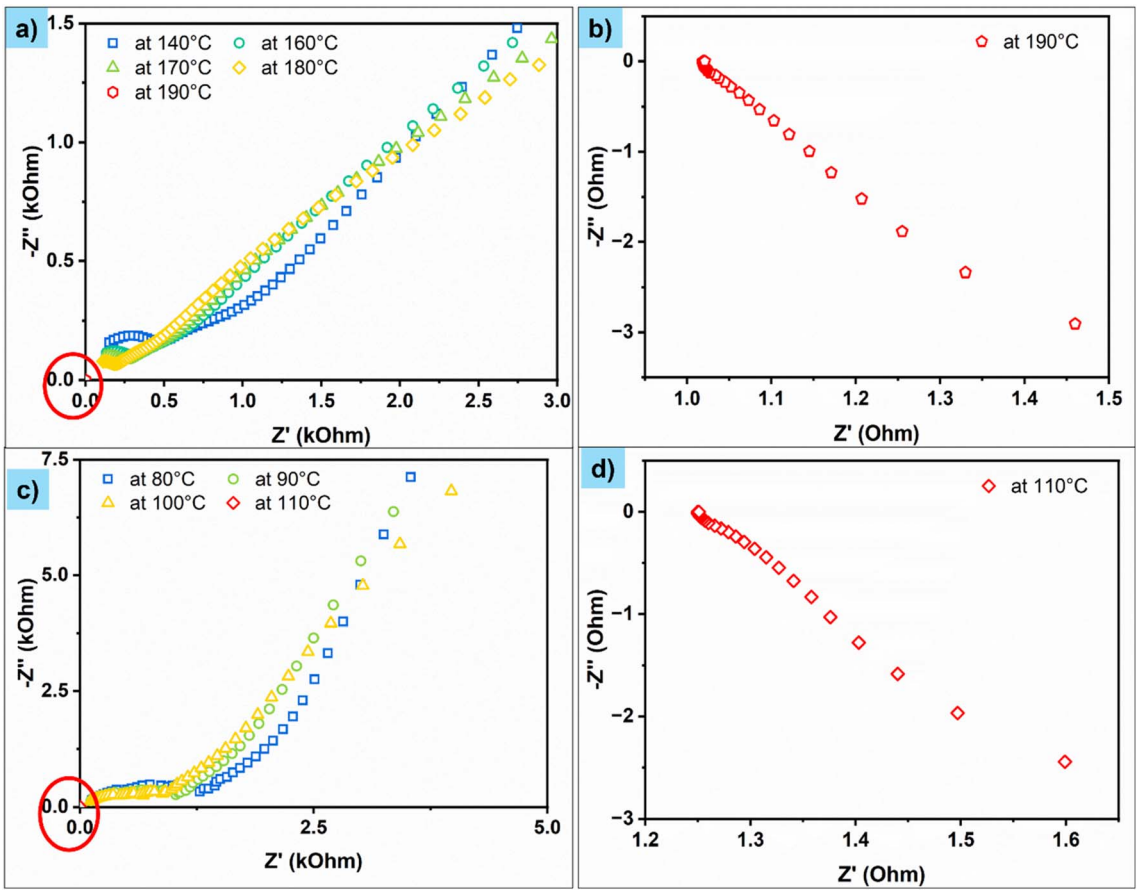

Fig. 3 (a) Impedance spectra of the Al–NMC/LLZO/Li–Cu cell in the temperature range of 140 °C to 190 °C with increments of +10 °C; (b) impedance spectra of the Al–NMC/LLZO/Li–Cu cell at 190 °C; (c) impedance spectra of the Al–NMO/NGS/Na–Al cell in the temperature range of 80 °C to 110 °C with increments of +10 °C; (d) impedance spectra of the Al–NMO/NGS/Na–Al cell at 110 °C. The red circles in (a) and (c) highlight the impedance falling below 2 Ω after short-circuiting occurs.

behaviour was observed when the cells were short-circuited. This confirms that a shunt is formed when a short circuit occurs in these cells. We also observed this kind of impedance behaviour in short-circuited symmetrical cells (Al–Na/BASE/Na–Al) after depositing and stripping Na at 0.4 mA (Fig. S2†). The short circuit in this cell was due to Na dendrite formation and puncturing; therefore, low resistance paths were generated.

Half cells and anode-free cells

Following symmetrical cells, we demonstrated the short-circuiting behaviour in half-cells. The impedance spectra of the Al–NMC/LLZO/Li–Cu and Al–NMO/NGS/Na–Al cells are shown in Fig. 3a and c. The impedance spectra of the additional half-cell (Al–NMO/LBASE/Na–Al) are shown in Fig. S3.† Similar to the symmetrical cells, the half cells are short-circuiting when Li and Na metals melt. The impedance fell below 2 Ω when the short-circuit occurred (Fig. 3b and d). A shunt-type resistor forms when the cells are short-circuited, similar to symmetrical cells. We fabricated anode-free cells and charged them to deposit Na on the anode current collector (Al foil). Na was deposited on the opposite side of the NGS disc, as evidenced visually, but only a small amount of Na was deposited (Fig.-S4a†). This would be too little to flow in the cell and cause a short circuit (particularly with a 1 mm thick NGS disc). Unfortunately, we could not deposit a significant amount of Na, probably due to the lack of applied pressure. We could not load more than 20 mg of the active material over 12 mm diameter NGS discs to maximise the amount of Na deposited (our attempt to coat more than 20 mg of NMO resulted in the peeling of the cathode layer from the solid electrolyte disc). Interestingly, the cell's impedance changed after charging the battery due to Na deposition (Fig. S4b†). The impedance spectra of the initial anode-free cell (Al–NMO/NGS/Al) consist of an inclined line at a lower frequency. The inclined line disappeared after charging, confirming sodium deposition between the NGS and Al interface. However, we reckon that the anode-free cells are identical to half cells after the first charge. Therefore, the half-cell results can be extended to anode-free cells.

Additional evidence of short-circuiting is provided through direct visualisation *via operando* digital microscopy experiments. The experimental setup is shown in Fig. S5.† The optical images of the symmetrical cell (Al–Na/NGS/Na–Al) recorded at various temperatures are shown in Fig. 4a–c. No visual changes

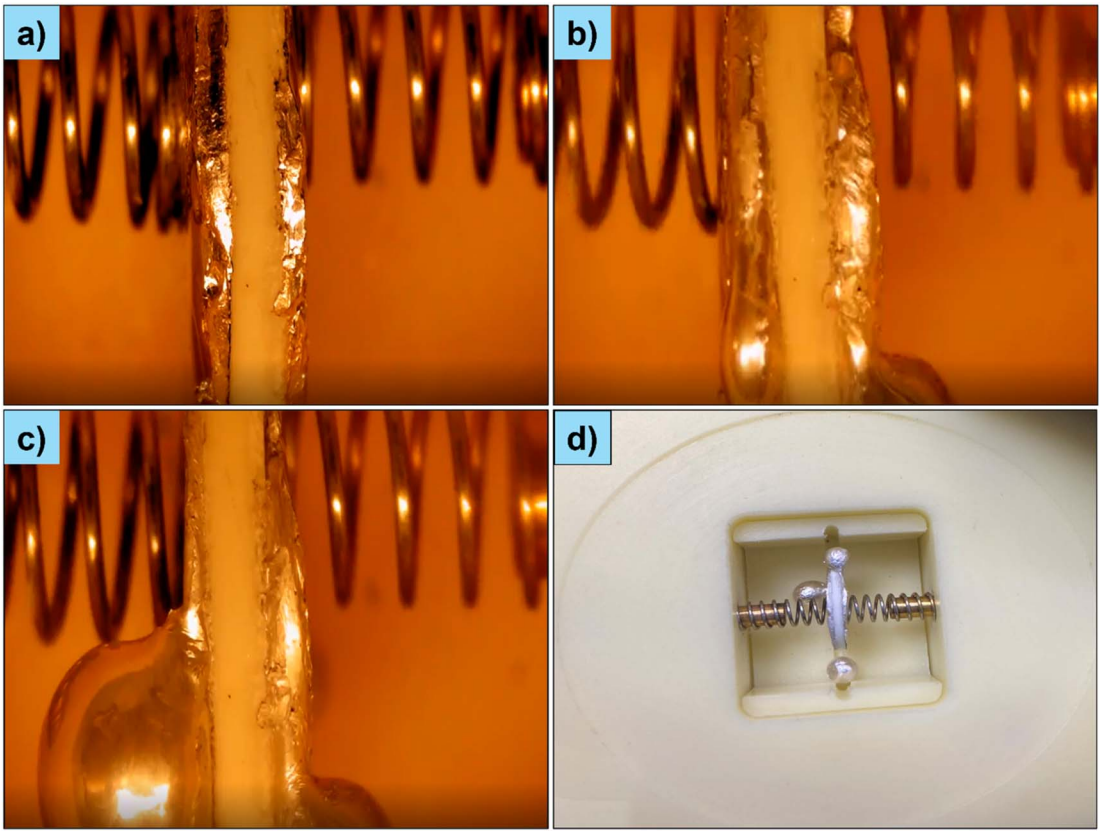

Fig. 4 Optical images of the symmetrical cell (Al–Na/NGS/Na–Al) at various temperatures: (a) at 80 °C, (b) at 110 °C, and (c) at 120 °C. (d) Digital images of the optical cell were recorded at RT after cooling down the cell and heating it to 120 °C (this cell is different from those used in (a)–(c)). The optical cell was placed in a digital dry block heater, which can be heated up to 120 °C. After closing the heater with a transparent lid, its temperature was raised to 80 °C, followed by a step-by-step increase from 80 °C to 120 °C (by +10 °C). Dwell time is approximately 10 minutes at each step. Digital images were recorded, and videos were recorded for each step. All these measurements were performed inside a glove box as our optical cell was not leakproof beyond 60 °C. The digital image of the experimental setup is shown in Fig. S5.†

were seen in the cell below 100 °C. However, Na started melting above 100 °C. The video of the cell recorded at a temperature of 110 °C is given in Fig. S6.† Na was seen melting at 110 °C, and beyond 110 °C, Na melt turned into spheres. Similar observations are made with half cells. The results of the half cell (Al–NMO/BASE/Na–Al) are given in Fig. S7.† The video of the cell recorded at a temperature of 110 °C is given in Fig. S8.† The short-circuit occurred between 100 °C and 110 °C in the symmetrical and half-cells. We hypothesise that Na melt was forming at these temperatures, flowing through the cracks and pores of the solid electrolyte and resulting in short-circuiting. Beyond 110 °C, Na melt turns into spheres and short-circuits over the surface (Fig. 4c and d). By combining the results from the impedance experiments and *operando* microscopy visual experiments, we conclude that the short circuiting occurs initially through the flow of melt through the pores of the solid electrolyte and subsequently over the surface when the temperature increases further.

Conclusion and perception

In conclusion, we showed that using Li and Na metals as anode materials in batteries might lead to an issue. When the temperature of the cells using Li and Na metals as anodes reaches the value of their melting points, these batteries will short-circuit internally and fail. Considering the high electronic conductivity and liquid nature of the Li and Na melts, the internal short circuits will initiate exothermic reactions, quickly releasing large amounts of energy. This could lead to severe damaging effects. While the Li metal melting temperature of 180.5 °C is not reached commonly, the Na metal melting temperature of 98 °C could be reached more often in batteries (particularly internally). Besides, Na metal reacts more violently with the atmosphere. Therefore, the Na metal as an anode in commercial batteries is more vulnerable. Batteries using any electrically conducting and low melting point electrode materials should be avoided. Batteries with open electrolyte design are unsuitable for electrically conducting flowable electrodes. However, adopting a sealed electrolyte design like that in ZEBRA and Na–S batteries might enable using these metals as anodes. Alternatively, LIBs and SIBs can continue to use much safer carbon-based anode materials (or other safer materials) in commercial batteries. Even with carbon-based anodes, we suggest avoiding fast charging to avoid potential metal deposition. However, unlike typical LIBs and SIBs, anode-free

batteries must use alkali metal anodes deposited in the first charge. Therefore, this concept is more worrisome.

Methods

Na-β″-Alumina (BASE) and Li-β″-alumina (LBASE) discs of 12 mm in diameter and 1 mm thick were obtained from Ionotec Ltd, England. $Li_{6.4}La_3Zr_{1.4}Ta_{0.6}O_{12}$ (LLZO) powder was obtained from MSE suppliers (Ampcera™). $LiNi_{0.8}Mn_{0.1}Co_{0.1}O_2$ (NMC), PVDF, NMP, Super P, Li metal, Al metal, and Cu metal foil were obtained from the Gelon Lib Group, China. Na sticks covered in protective hydrocarbon oil were used to prepare Na-based cells (99% Alfa Aesar). A small split cell with a quartz window (EQ-STC-SSI) was used and purchased from MTI, USA, for optical microscope experiments. The as-received LLZO powder was milled at 400 rpm for 12 h, pressed into 12 mm diameter discs and sintered at 1050 °C for 8 h. The sintered discs were used for further measurements. $Na_5GdSi_4O_{12}$ (NGS) and P2-type $Na_{0.7}Mn_{0.9}Mg_{0.1}O_2$ (NMO) were synthesised according to our previous reports.[20,21] A Fritsch Pulverisette 6 was used for ball milling experiments (ZrO_2 vials (80 mL), and 10 mm balls were used for milling). The phase purity of the synthesised and received samples was determined *via* XRD using a Bruker D8 Discover diffractometer and Cu Kα radiation (40 kV; 40 mA). All electrochemical measurements were performed using a Gamry 1010E potentiostat. Gold was sputtered as an ion-blocking electrode on either side of the solid electrolyte discs using an Agar sputter coater for ionic conductivity measurements. The electrochemical impedance spectroscopy (EIS) spectrum was subsequently recorded on these gold-coated solid electrolytes between 1 MHz and 0.1 Hz. Ionic conductivities were derived by fitting the resulting EIS spectra.

To fabricate Li-based symmetric cells, the surface of Li foil was mechanically cleaned using a scalpel blade to expose fresh Li and cut as discs (the same size as the diameter of the solid electrolyte discs). These Li–metal electrodes were placed on both sides of the solid electrolyte discs. The other side of Li-discs was covered with Cu-foil. The Cu–Li/solid electrolyte/Li–Cu stack was pressed by hand. The Cu–Li/solid electrolyte/Li–Cu sandwiched solid electrolyte discs were transferred to a modified Swagelok cell and placed between two stainless-steel (SS) current collectors. The top part of the SS current collector was compressed with an SS spring (the compression force of the spring is 40 N) using an SS tightening rod. NMC was used as the cathode material to make half-cells and anode-free cells. A slurry was made of an NMC + Super P + PVDF (80 wt% + 8 wt% + 12 wt%) mixture, and NMP was hand coated on LLZO discs with a spatula and dried at 120 °C overnight. These dried pellets were used to make half-cells and anode-free cells. The cathode layer contains approximately 20 mg of NMC. To make half-cells (Al–NMC/LLZO/Li–Cu), the uncoated side of the solid electrolyte discs was pressed with Li metal, as was the case for symmetrical cells.

To fabricate Na-based symmetric cells, a clean piece of Na metal was cut from a rod pressed flat and cut into circular electrodes. Their surface was mechanically cleaned using a scalpel blade to expose fresh sodium. The Na–metal electrodes were placed on both sides of the BASE or NGS pellets. The other side of Na-discs was covered with Al-foil. The Al–Na/BASE/Na–Al or Al–Na/NGS/Na–Al stack was pressed by hand. The other fabrication and measurement conditions were similar to those of Li symmetrical cells. NMO was used as the cathode material to make half-cell and anode-free cells. To make SIB half cells and anode-free cells, a slurry was made of an NMO + Super P + PVDF (80 wt% + 8 wt% + 12 wt%) mixture, and NMP was hand coated on BASE or NGS discs with a spatula and dried at 120 °C overnight. The cathode layer contains approximately 20 mg of NMO. To make half-cells (Al–NMO/BASE/Na–Al or NMO/NGS/Na–Al), the uncoated side of the solid electrolyte discs was pressed with Na metal, as it was in the case of symmetrical cells. Then, both sides of the discs were covered with Al foil. The NMO-coated discs were covered on both sides with Al foil (to make anode-free cells (Al–NMO/BASE/Al or Al–NMO/NGS/Al)). All testing and measurements were done in modified Swagelok cells. The design of the modified Swagelok cell was discussed in our previous publications.[22] The modified Swagelok cells were assembled inside an MBraun glovebox (O_2 < 0.5 ppm, H_2O < 0.5 ppm).

Data availability

The data supporting this article have been included as part of the ESI.†

Author contributions

MAR conceived the idea and wrote the full manuscript. AM performed the experiments, and MAR and AM analysed the data.

Conflicts of interest

The authors declare no competing financial interest.

References

1 R. Wang, W. Cui, F. Chu and F. Wu, Lithium Metal Anodes: Present and Future, *J. Energy Chem.*, 2020, **48**, 145–159, DOI: **10.1016/j.jechem.2019.12.024**.
2 D. Puthusseri, M. Wahid and S. Ogale, Recent Advances in Understanding the Formation and Mitigation of Dendrites in Lithium Metal Batteries, *Energy Fuels*, 2021, **35**(11), 9187–9208, DOI: **10.1021/acs.energyfuels.1c00643**.
3 Y. Huang, H. Yang, Y. Gao, G. Chen, Y. Li, L. Shi and D. Zhang, Mechanism and Solutions of Lithium Dendrite Growth in Lithium Metal Batteries, *Mater. Chem. Front.*, 2024, **8**(5), 1282–1299, DOI: **10.1039/D3QM01151H**.
4 J. Asenbauer, T. Eisenmann, M. Kuenzel, A. Kazzazi, Z. Chen and D. Bresser, The Success Story of Graphite as a Lithium-Ion Anode Material – Fundamentals, Remaining Challenges, and Recent Developments Including Silicon (Oxide) Composites, *Sustainable Energy Fuels*, 2020, **4**(11), 5387–5416, DOI: **10.1039/D0SE00175A**.

5 H. Zhang, Y. Yang, D. Ren, L. Wang and X. He, Graphite as Anode Materials: Fundamental Mechanism, Recent Progress and Advances, *Energy Storage Mater.*, 2021, **36**, 147–170, DOI: **10.1016/j.ensm.2020.12.027**.

6 Y. Jin, B. Zhu, Z. Lu, N. Liu and J. Zhu, Challenges and Recent Progress in the Development of Si Anodes for Lithium-Ion Battery, *Adv. Energy Mater.*, 2017, **7**(23), 1700715, DOI: **10.1002/aenm.201700715**.

7 T. Krauskopf, F. H. Richter, W. G. Zeier and J. Janek, Physicochemical Concepts of the Lithium Metal Anode in Solid-State Batteries, *Chem. Rev.*, 2020, **120**(15), 7745–7794, DOI: **10.1021/acs.chemrev.0c00431**.

8 X. Zhang, A. Wang, X. Liu and J. Luo, Dendrites in Lithium Metal Anodes: Suppression, Regulation, and Elimination, *Acc. Chem. Res.*, 2019, **52**(11), 3223–3232, DOI: **10.1021/acs.accounts.9b00437**.

9 L. He, Q. Sun, L. Lu and S. Adams, Understanding and Preventing Dendrite Growth in Lithium Metal Batteries, *ACS Appl. Mater. Interfaces*, 2021, **13**(29), 34320–34331, DOI: **10.1021/acsami.1c08268**.

10 R. J.-Y. Park, C. M. Eschler, C. D. Fincher, A. F. Badel, P. Guan, M. Pharr, B. W. Sheldon, W. C. Carter, V. Viswanathan and Y.-M. Chiang, Semi-Solid Alkali Metal Electrodes Enabling High Critical Current Densities in Solid Electrolyte Batteries, *Nat. Energy*, 2021, **6**(3), 314–322, DOI: **10.1038/s41560-021-00786-w**.

11 W. Shao, H. Shi, X. Jian, Z.-S. Wu and F. Hu, Hard-Carbon Anodes for Sodium-Ion Batteries: Recent Status and Challenging Perspectives, *Adv. Energy Sustainability Res.*, 2022, **3**(7), 2200009, DOI: **10.1002/aesr.202200009**.

12 S. Tan, H. Yang, Z. Zhang, X. Xu, Y. Xu, J. Zhou, X. Zhou, Z. Pan, X. Rao, Y. Gu, Z. Wang, Y. Wu, X. Liu and Y. Zhang, The Progress of Hard Carbon as an Anode Material in Sodium-Ion Batteries, *Molecules*, 2023, **28**(7), 3134, DOI: **10.3390/molecules28073134**.

13 C. Zhao, Y. Lu, J. Yue, D. Pan, Y. Qi, Y.-S. Hu and L. Chen, Advanced Na Metal Anodes, *J. Energy Chem.*, 2018, **27**(6), 1584–1596, DOI: **10.1016/j.jechem.2018.03.004**.

14 Y. An, Y. Zeng, D. Luan and X. W. (David) Lou, Materials Design for High-Energy-Density Anode-Free Batteries, *Matter*, 2024, **7**(4), 1466–1502, DOI: **10.1016/j.matt.2024.02.012**.

15 Y. Tian, Y. An, C. Wei, H. Jiang, S. Xiong, J. Feng and Y. Qian, Recently Advances and Perspectives of Anode-Free Rechargeable Batteries, *Nano Energy*, 2020, **78**, 105344, DOI: **10.1016/j.nanoen.2020.105344**.

16 W. Yao, P. Zou, M. Wang, H. Zhan, F. Kang and C. Yang, Design Principle, Optimization Strategies, and Future Perspectives of Anode-Free Configurations for High-Energy Rechargeable Metal Batteries, *Electrochem. Energy Rev.*, 2021, **4**(3), 601–631, DOI: **10.1007/s41918-021-00106-6**.

17 Z. Xie, Z. Wu, X. An, X. Yue, J. Wang, A. Abudula and G. Guan, Anode-Free Rechargeable Lithium Metal Batteries: Progress and Prospects, *Energy Storage Mater.*, 2020, **32**, 386–401, DOI: **10.1016/j.ensm.2020.07.004**.

18 N. Narayana and D. R. Burgess Jr, *Melting Points and Boiling Points for the Alkali Metals*, NIST TN 2273, 2024, DOI: **10.6028/NIST.TN.2273**.

19 D. Velumani and A. Bansal, Thermal Behavior of Lithium- and Sodium-Ion Batteries: A Review on Heat Generation, Battery Degradation, Thermal Runway – Perspective and Future Directions, *Energy Fuels*, 2022, **36**(23), 14000–14029, DOI: **10.1021/acs.energyfuels.2c02889**.

20 A. Michalak, S. Behara and M. Anji Reddy, Reinvestigation of $Na_5GdSi_4O_{12}$: A Potentially Better Solid Electrolyte than Sodium β Alumina for Solid-State Sodium Batteries, *ACS Appl. Mater. Interfaces*, 2024, **16**(6), 7112–7118, DOI: **10.1021/acsami.3c16153**.

21 V. Pamidi, S. Trivedi, S. Behara, M. Fichtner and M. A. Reddy, Micron-Sized Single-Crystal Cathodes for Sodium-Ion Batteries, *iScience*, 2022, **25**(5), 104205, DOI: **10.1016/j.isci.2022.104205**.

22 I. Mohammad, R. Witter, M. Fichtner and M. Anji Reddy, Room-Temperature, Rechargeable Solid-State Fluoride-Ion Batteries, *ACS Appl. Energy Mater.*, 2018, **1**(9), 4766–4775, DOI: **10.1021/acsaem.8b00864**.